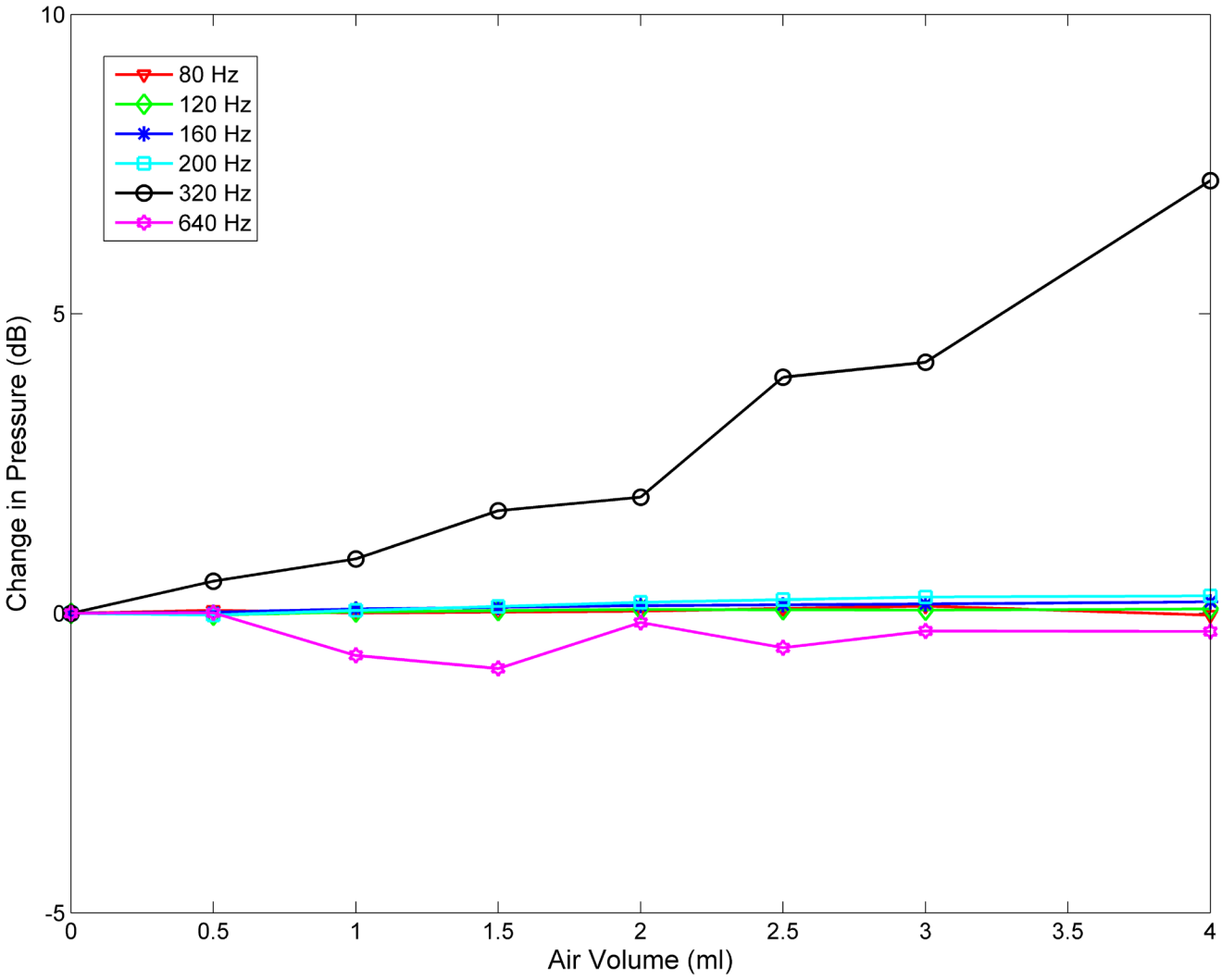

Figure S1. Effect of air on the sound pressure in the standing wave tube at high particle motion-to-pressure depth. The overall sound field was affected by introduction of air to the standing wave tube. Here the change in pressure (pressure measured with air volume in the tube relative to pressure measured without air volume in the tube) is plotted as a function of air introduced in depth with high particle motion-to-pressure ratio at frequencies used.

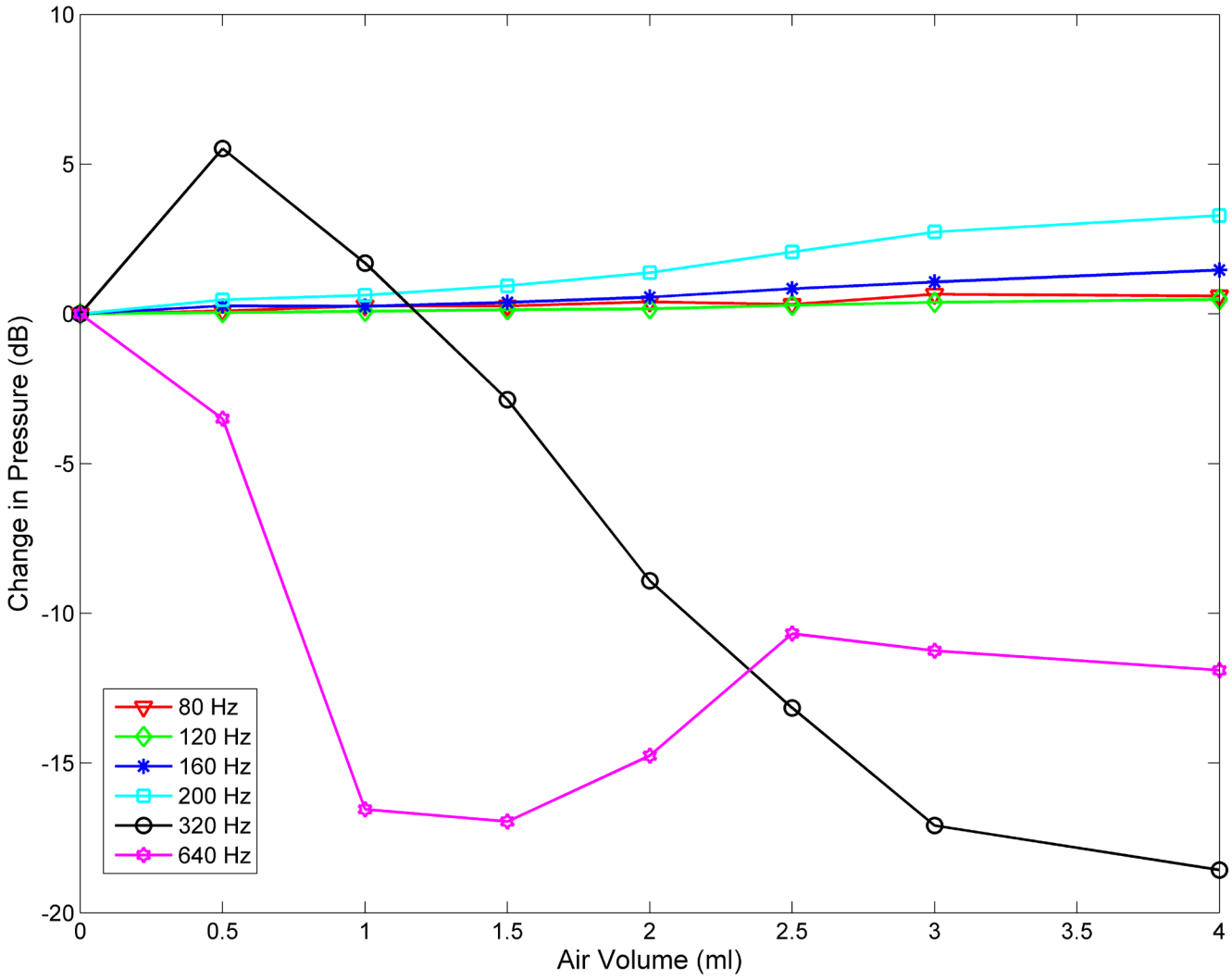

Figure S2. Effect of air on the sound pressure in the standing wave tube at low particle motion-to-pressure depth. The overall sound field was affected by introduction of air to the standing wave tube. Here the change in pressure (pressure measured with air volume in the tube relative to pressure measured without air volume in the tube) is plotted as a function of air introduced in depth with low particle motion-to-pressure ratio at frequencies used.

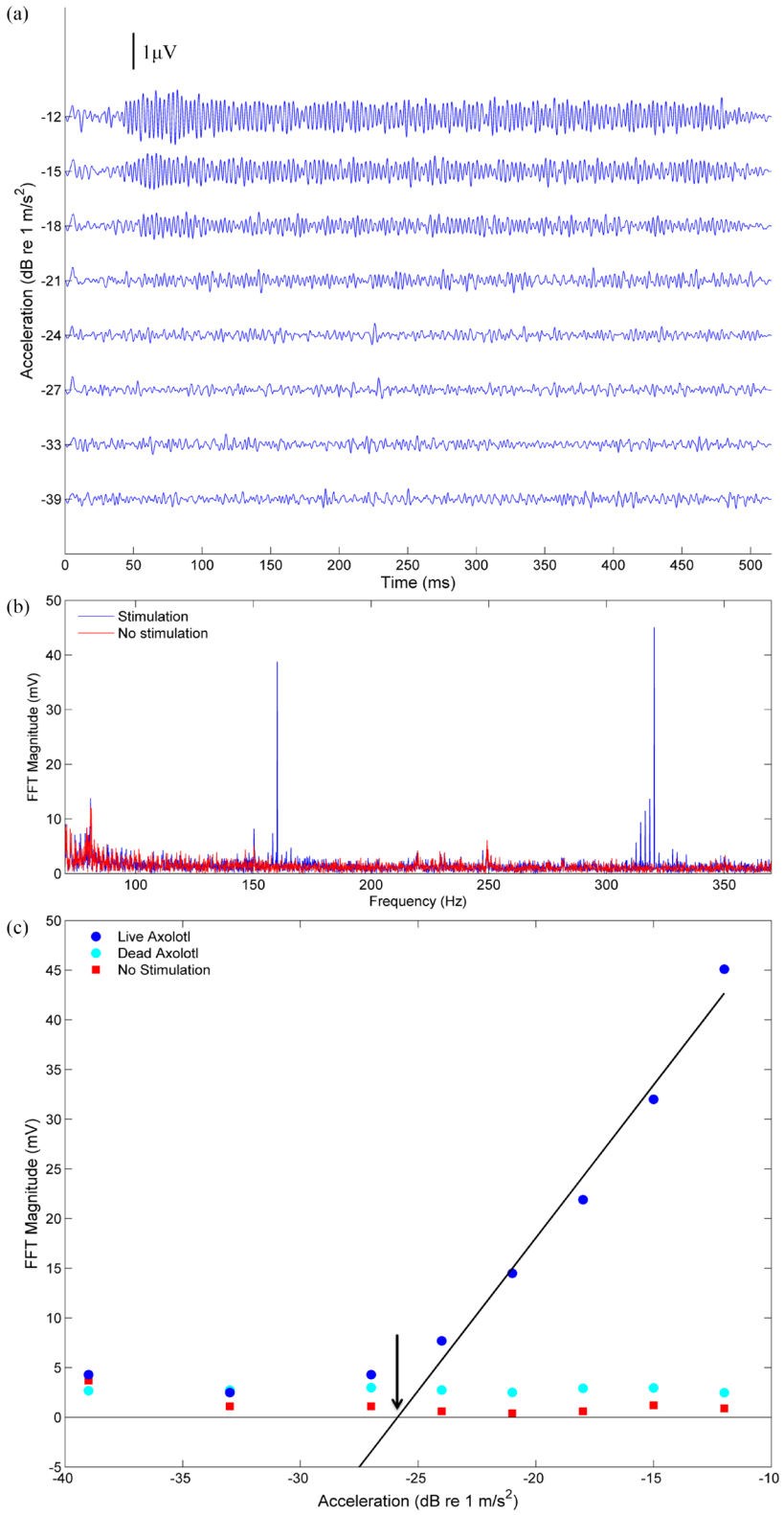

Figure S3. Neural response to 160 Hz pure tone stimuli of increasing intensity. Pure tone stimulation resulted in characteristic signal in the evoked potentials at twice the stimulation frequency which was used to determine sensitivity thresholds. a) Average neural response underwater to 160 Hz pure tones, band pass filtered at 100 and 400 Hz by a second-order Butterworth filter b) FFT of the neural response to 160 Hz tone of -12 dB re 1 m/s2 (blue) and to no stimulation (red). The FFT of the neural response to tone stimulus show a significant peak at twice the stimulation frequency, whereas the FFT of the neural response to no stimulation contain no such peak. c) AEP response as a function of acceleration stimulation. The FFT peak size at the second harmonic of the combined AEP response was found to increase with increasing stimulation intensity for tone stimulation (Blue dots), but not for periods of no stimulation (Red squares) in live animals. In comparison, no increase was seen in a dead axolotl used as control (Cyan dots). Thresholds were defined as the zero-crossing of the regression line as indicated by the arrow.

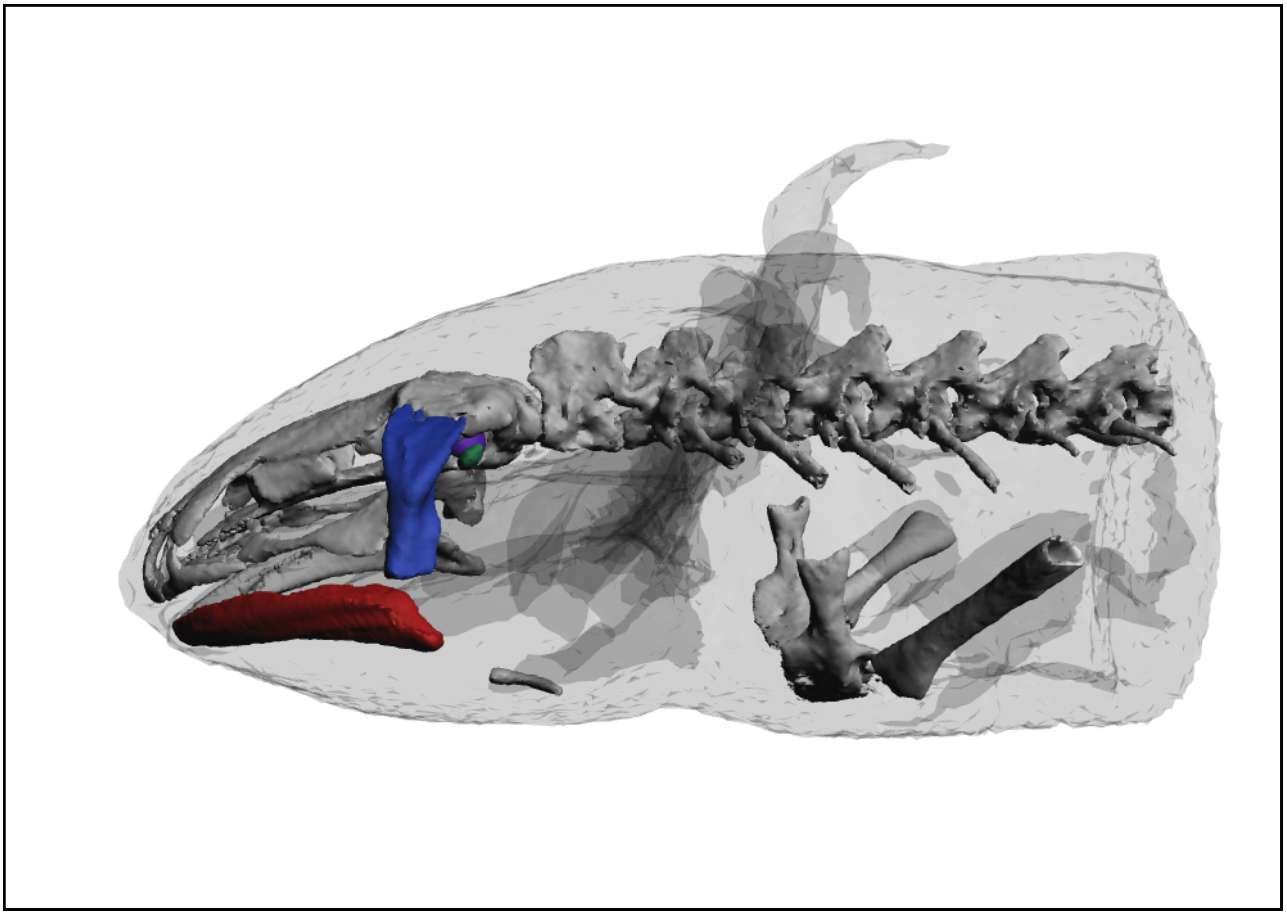

Figure S4. Interactive three-dimensional model of juvenile axolotl skull and inner ear. Click to activate the model. Red: Mandible, Blue: Quadrate, Green: Columella Auris, Purple: Saccule and Pink: Opercularis and levator scapulae muscles. Segmentation and modelling were accomplished in Amira 5.6 (Visage Imaging, Berlin, Germany) and Adobe Acrobat 3D Toolkit (San Jose, California, USA). Use the tools in the 3D menu to manipulate the model. The different components can be highlighted using the modeltree.

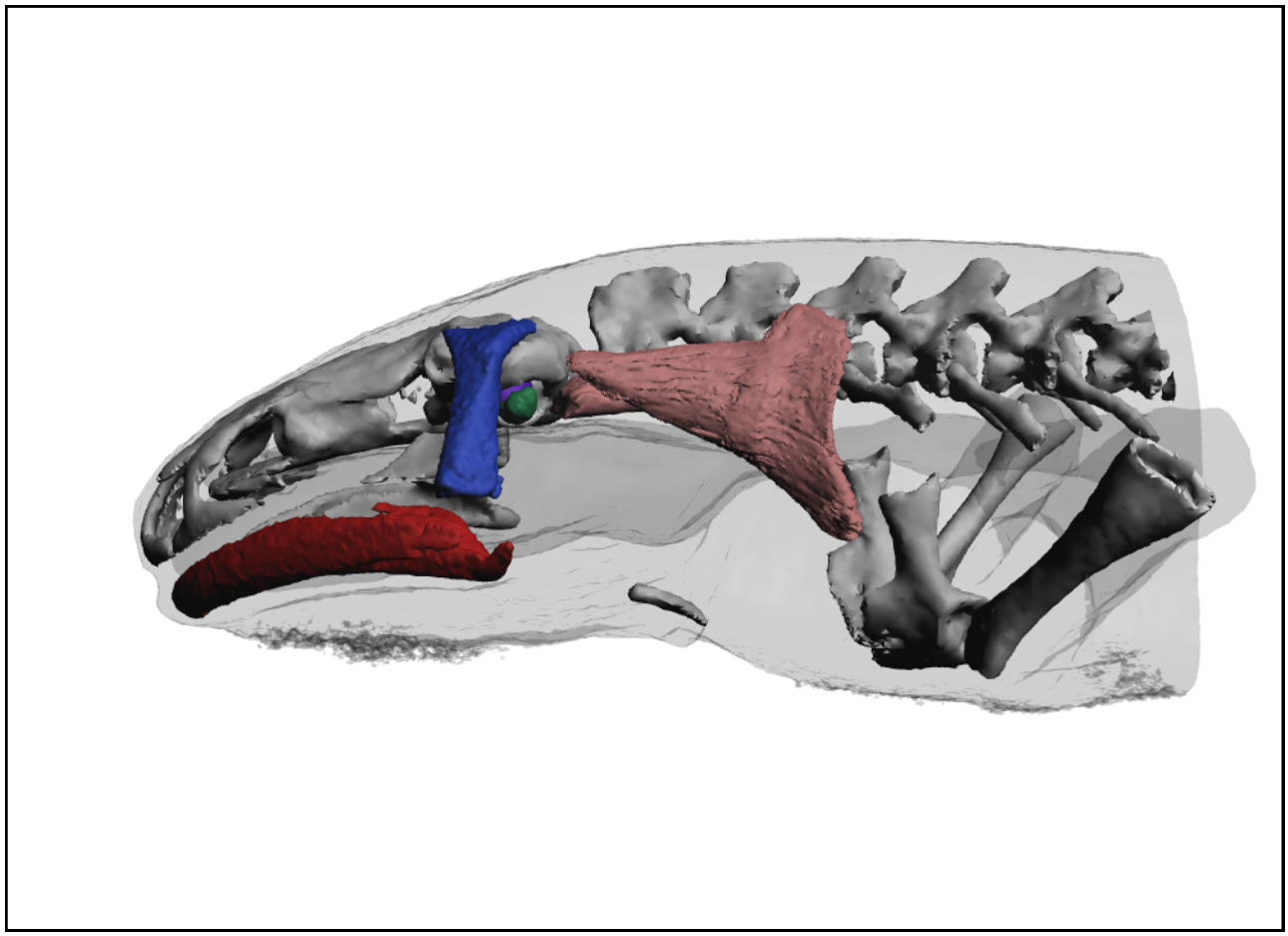

Figure S5. Interactive three-dimensional model of adult axolotl skull and inner ear. Click to activate the model. Red: Mandible, Blue: Quadrate, Green: Columella Auris, Purple: Saccule and Pink: Opercularis and levator scapulae muscles. Segmentation and modelling were accomplished in Amira 5.6 (Visage Imaging, Berlin, Germany) and Adobe Acrobat 3D Toolkit (San Jose, California, USA). Use the tools in the 3D menu to manipulate the model. The different components can be highlighted using the modeltree.

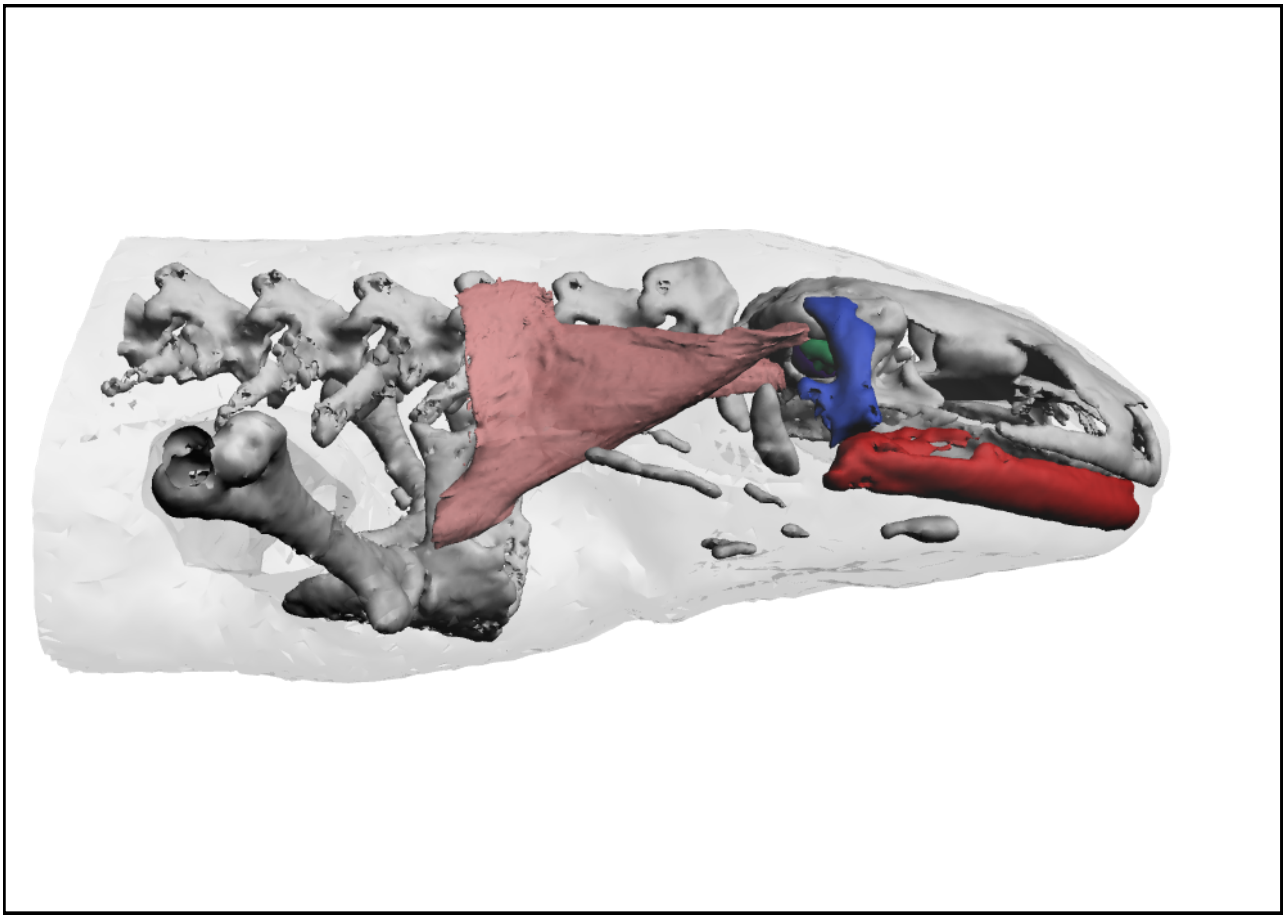

Figure S6. Interactive three-dimensional model of adult tiger salamander skull and inner ear. Click to activate the model. Red: Mandible, Blue: Quadrate, Green: Columella Auris, Purple: Saccule and Pink: Opercularis and levator scapulae muscles. Segmentation and modelling were accomplished in Amira 5.6 (Visage Imaging, Berlin, Germany) and Adobe Acrobat 3D Toolkit (San Jose, California, USA). Use the tools in the 3D menu to manipulate the model. The different components can be highlighted using the modeltree.